Characterization of Polymer Nanocomposite Interphase and Its Impact on Mechanical Properties

Dan Ciprari,[†] Karl Jacob,[‡,§] and Rina Tannenbaum*[,†]

School of Materials Science and Engineering, School of Polymer, Textile and Fiber Engineering, and G.W.W. Woodruff School of Mechanical Engineering, Georgia Institute of Technology, Atlanta, Georgia 30332

Received January 30, 2006; Revised Manuscript Received July 2, 2006

ABSTRACT: The structure of the interphase, a region between nanoparticle fillers and the bulk polymer matrix in a particle reinforced composite, was investigated using two different approaches. The polymer nanocomposite systems consists of alumina (Al_2O_3) and magnetite (Fe_3O_4) nanoparticles embedded in poly(methyl methacrylate) (PMMA) and polystyrene (PS) matrices. The first approach utilized data from thermal gravimetric analysis (TGA) and transmission electron microscopy (TEM) to predict the structure and density of the interphase for four nanocomposite systems. In the second approach, the nature of bonding between the polymer and the nanoparticle surfaces was analyzed using Fourier transform infrared spectroscopy (FTIR) to calculate the density of the interphase for two PMMA-based nanocomposite systems. Mechanical properties of these composites were correlated with the structure of the interface, and results from the two approaches were compared with previous studies. Moreover, by comparing results from the two characterization approaches, a new method for characterizing the degree of nanoparticle flocculation in a composite is also provided. The results indicate that Al_2O_3 nanoparticles are more reactive with the polymer matrix than Fe_3O_4 nanoparticles, but neither have strong interactions with the matrix, a fact that leads to low-density interphase and consequently results in more compliant composites. Tensile testing, dynamic mechanical analysis (DMA), and nanoindentation tests confirmed that these nanocomposite systems do not have the same mechanical properties as their respective pure polymer systems.

1. Introduction

A polymer nanocomposite is a polymer matrix with a reinforcing phase consisting of particles with one dimension in the nanosized regime. In the past decade, extensive research has focused on polymer nanocomposites in hopes of exploiting the unique properties of materials in the nanosized regime.[1−6] A general conclusion has been drawn that nanocomposites show much improved mechanical properties over similar microsized systems.[2,3,5−10] Because of their small size, nanoparticles have a high surface-to-volume ratio and provide high-energy surfaces. A desirable result of embedding nanoparticles into a polymer matrix is the enhanced bonding between the polymer matrix and filler, resulting from the nanoparticles' high interfacial energy.[2,5,7,11] Classical composite theory predicts that improved bonding between the polymer matrix and the reinforcing phase leads to improved mechanical properties.[2,5,7,11,12]

Despite these predictions, however, mechanical tests of nanocomposites have shown mixed results.[1,13,14] Although some research has shown great improvement of mechanical properties for nanocomposites compared to composites with particles with length scales in the microrange,[1,2,7] those results have not been consistent.[1,5,13,15] No clear conclusions have been made regarding trends in the mechanical properties of polymer nanocomposites,[1,5,13] as current polymer models have not been able to consistently predict the properties of nanocomposites.[1,5,16−19] Polymer composite theories in the past have relied on the idea that the modulus of a composite is a function of the mismatch of properties of constituents, volume fraction, shape and arrangement of inclusions, and matrix-inclusion interface.[4,5,7,13] These theories, therefore, predict that the effect on the composite system is independent of the size of the inclusion. Recent theories have included the size of the filler particulate to predict the properties of composites.[2,6,7,11,13,19−24]

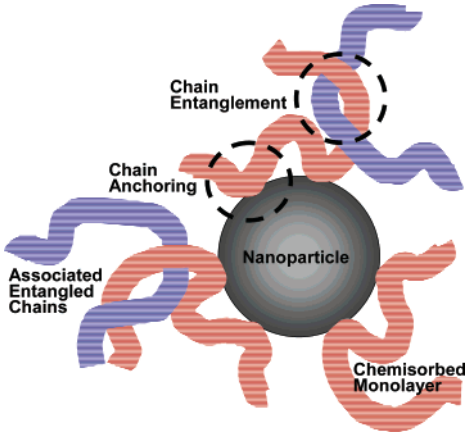

Figure 1. Schematic representation of the interphase region between a filler and a polymer matrix.

An area of polymer composite structure that has always garnered attention is the region near the interface of the polymer matrix and the filler.[1,7,10,11,14,20,25−27] Despite the large variety of polymer composite systems, a common thread among all the systems is the existence of a phase border between the matrix and filler and the formation of an interphase layer between them.[7,11,25,26,28] As seen in Figure 1, the interphase layer extends well beyond the adsorption layer of the matrix chains bound to the filler surface. The structure of the interphase is different than either the filler or matrix phases, and it varies depending on the distance from the bound surface.

Because of the differences in structure, properties of the polymer at the interface can differ dramatically from the bulk polymer.[7,24−26] The interphase structure and properties are

* Corresponding author. E-mail: rina.tannenbaum@mse.gatech.edu.
† School of Materials Science and Engineering.
‡ School of Polymer, Textile and Fiber Engineering.
§ G.W.W. Woodruff School of Mechanical Engineering.

10.1021/ma0602270 CCC: $33.50
Published on Web 08/18/2006

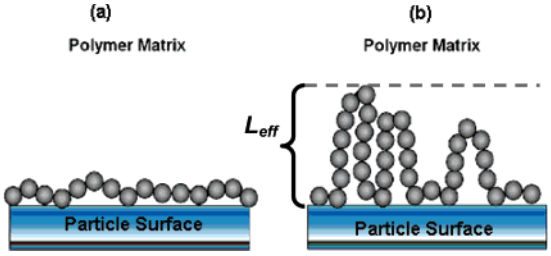

Figure 2. Schematic representation of the adsorption characteristics of polymer chains onto the surface of metal oxide clusters in a metal−polymer nanocomposite: (a) a strongly binding polymer adheres to the surface and most of the segments reside on the surface and (b) a weakly binding polymer adheres to the surface and most of the segments reside in loops.

important to the overall mechanical properties of the composite because its distinct properties control the load transfer between matrix and filler.[15,17,20,25,26] The concept of interphase is not unique to nanocomposites, but because of the large surface area of nanoparticles, the interphase can easily become the dominating factor in developing the properties of nanocomposites.[7,24,25] A 1 nm thick interface surrounding microparticles in a composite represents as little as 0.3% of the total composite volume. However, a 1 nm thick interface layer on nanoparticles can reach 30% of the total volume.[7] As shown in Figure 1, the interphase has a characteristic structure consisting of flexible polymer chains, typically in sequences of adsorbed segments (point contacts, i.e., anchors, or trains) and unadsorbed segments, such as loops and tails, which in turn are entangled with other chains in their proximity and which are not necessarily bound to the surface. Interphase thickness for a specific particle−polymer system is not a constant size because the interphase has no well-defined border with the bulk polymer.[28] The effective value of the thickness depends on chain flexibility, the energy of adsorption, and the extent of chain entanglements, which are determined by the surface energies of the polymer and the nanoparticles. Because of conformational limitations brought by particles in addition to other restrictions on chain conformation, only a relatively small number of segments within a chain are directly bound to the surface.[28] If all areas of the surface are capable of adsorption, then polymer segments, for a reasonably flexible polymer chain, are readily adsorbed on the surface, resulting in short loops and a flat (i.e., dense) layer close to the surface, as shown in Figure 2a. If the chain segments have weak interaction with the surface or if the chain is rigid, the loops and tails extend farther into the matrix and form a region of lower density, as shown in Figure 2b.[26] Therefore, the strength of the interaction of a polymer molecule with the surface of the nanoparticles controls both the polymer molecular conformations at the surface and the entanglement distribution in a larger region surrounding the nanoparticle. Hence, a higher degree of entanglements will result in a larger number of polymer chains that are associated with a given nanoparticle, of which only a fraction are actually anchored to the surface.

In this work we characterized the mechanical properties of four polymer nanocomposite systems and investigated the role of the interphase structure on their behavior. Alumina (Al_2O_3) and magnetite (Fe_3O_4) nanoparticles were dispersed in polystyrene (PS) and poly(methyl methacrylate) (PMMA) matrices. Appropriate samples were created to support mechanical characterization using tensile testing, dynamic mechanical analysis (DMA), and nanoindentation. Interphase bonding, interphase density, and thickness were quantified using Fourier transform infrared spectroscopy (FTIR), transmission electron microscopy (TEM), and thermal gravimetric analysis (TGA). Alumina (39 nm) nanoparticles and magnetite (90 nm) were chosen on the basis of availability and size distribution and due to the existence of results from literature for comparison.[15,29−31]

PMMA and PS were chosen as the matrix materials on the basis of their differing reactivity with metal oxides. Previous studies have shown that PMMA adsorbs strongly to metal oxide nanoparticles through coordination of the carbonyl functional group to the metal surface sites. PS adsorbs weakly through dipole−dipole interactions between the π-electrons of the pendant benzene ring and the metal surface sites.[32] High molecular weight polymers with $\bar{M}_W$ = 350 000 g/mol were chosen to maximize chain flexibility, which facilitates chain adherence to a nanoparticle surface.[26,28] Filler volume fraction of 5% was chosen for all systems because it offers more opportunities for comparison to other studies.[1,2,15] To provide good solvents for the polymers, chlorobenzene was chosen for the PMMA systems and toluene was chosen for all PS systems.

2. Experimental Methods

2.1. Preparation of Initial System Mixture. PS−Fe_3O_4 samples were created as follows: 351 mL of toluene (Fisher Scientific, density 0.867 g/cm^3) was introduced into a 500 mL Erlenmeyer flask, which was placed on a Thermolyne Mirak stirring hot plate with the temperature set to 70 °C. A magnetic stirrer was dropped into the flask and began spinning at the preset speed of 200 rpm. 45.67 g of PS (Aldrich Chemical Co., Inc., $\bar{M}_W$ of 350 000 g/mol, density 1.040 g/cm^3) was poured into the flask. After the polymer was completely dissolved, the stirrer was removed. 0.49 g of magnetite (Fe_3O_4) nanoparticles (University of Illinois, D_{avg} = 90 nm, density 5.15 g/cm^3) was measured and kept in weighing paper. The flask was agitated on a Scientific Industries Vortex-2 Genie vortex with a setting of 8−10. While the mixture was swirling continuously the magnetite was slowly poured into the flask. Mixing continued for 5 min. The flask was covered with laboratory film and stored in a fume hood.

The four different polymer nanocomposite systems were created following the same procedures. PS−Al_2O_3 was created with 0.50 g of alumina (Al_2O_3) nanoparticles (Nanophase Technologies, D_{avg} = 39 nm, density 4.00 g/cm^3) in a solution of 36.54 g of PS dissolved in 281 mL of toluene. PMMA−Al_2O_3 was created using a similar procedure with 0.50 g of alumina in a solution of 32.48 g of PMMA (Aldrich Chemical Co., Inc., $\bar{M}_W$ of 350 000 g/mol, density 1.170 g/cm^3) dissolved in 220 mL of chlorobenzene (99+%, Acros, density 1.106 g/cm^3). PMMA−Fe_3O_4 was created with 0.44 g of Fe_3O_4 nanoparticles in 36.54 g of PMMA in 220 mL of chlorobenzene. Pure PS and PMMA reference samples were created using 36.33 g of PS in 140 mL of toluene and 32.48 g of PMMA in 110 mL of chlorobenzene.

2.2. Particle Characterization by TEM and SEM. Transmission electron microscopy (TEM) was used to determine the size and distribution of the original particles for all four polymer nanocomposite systems. TEM samples were obtained by placing a small droplet of the reacted solution containing the polymer-coated metal oxide particles onto a Formvar-coated copper TEM grid from Ted Pella. The grid rested on a thin piece of tissue paper so that the liquid would drain into the paper, leaving a very thin film on the grid itself. Additional samples were prepared by microtoming the sections used for SEM analysis and placed on similar Formvar-coated copper TEM grids. The TEM analysis was performed on a JEOL 4000EX high-resolution electron microscope with an operating voltage of 200 keV.

SEM was used to determine size and distribution of particles in tensile tested dogbone samples for all four polymer nanocomposite systems. After tensile testing, approximately a 5 mm section of the sample neck, including one fracture surface, was cut and placed on a SEM sample holder. The samples were sputter-coated with gold using an International Scientific Instruments sputter coater for 80 s to reduce charging. SEM was performed in a LEO 1530 Thermally-Assisted FEG scanning electron microscope at 10 kV.

2.3. Characterization of Interfacial Interactions. *2.3.1. Thermogravimetric Analysis.* Thermogravimetric analysis (TGA) was conducted to measure the thickness of the polymer interphase. TGA samples were prepared by centrifuging each of the four polymer nanocomposite mixtures using a Fisher Scientific Centrific model 228 centrifuge at 10 000−15 000 rpm for 12−17 min. The capped particles formed a solid mass at the bottom of the vial, and excess polymer and solvent solution were removed. The remaining particles were washed with solvent, and the vial was shaken using a Scientific Industries Vortex-2 Genie vortex for 1 min to remove any excess unbound polymer from the particles. The suspension was centrifuged again, and this process was repeated 3−4 times. The particles were placed onto a TGA platinum pan, and the data were collected using a TA Instruments Inc. TGA model 50 at a ramp rate of 10 °C/min to 600 °C.

2.3.2. Infrared Spectroscopy. FTIR was used to identify the bonding between the polymer matrix and nanoparticles in the two PMMA-based nanocomposites. The sample cell was placed into a Nicolet Instrument Corp. Nexus 870 FTIR spectrometer, and after the infrared sample compartment was sealed and purged for at least 5 min, a background spectrum was taken and assigned for use on subsequent spectral acquisitions. The vials containing the centrifuged capped particles were shaken using a Scientific Industries Vortex-2 Genie vortex to resuspend the particles. Using Nicolet OMNIC 5.2a software, the spectra of the capped metal oxide particles were compared against previously recorded spectra of PMMA solutions or PMMA thin films to highlight peaks unique to the capped particles.

2.4. Measurement of Mechanical Properties. Mechanical properties for all systems were characterized using tensile testing, dynamic mechanical analysis (DMA), and nanoindentation. Dog-bone-shaped samples were created following ASTM document D638 for tensile tests. The solution sample of the composite system was poured into the mold and left in a vacuum hood and then a dry oven for 24−72 h while solvent evaporated. This process was repeated for a total of 3−5 times or until the mold was filled. The sample was then placed in a Fisher Scientific Isotemp (model 281A) vacuum oven preheated to 120−140 °C with vacuum slowly raised to −28 in Hg. To remove air bubbles, each sample was compression-molded in a Carver compression-molding press with plates heated to 130−190 °C, increasing pressure periodically over a 1−3 h period up to a sustained pressure of 2000 psi for at least 1 h. Samples were allowed to cool in a compressed state. Tensile testing was performed using MTI Phoenix tensile testing equipment with a 10 000 lb load cell and a ±0.2 in. Instron extensometer with a loading rate corresponding to a 0.1 in/min displacement rate.

Thin film samples on glass slides were cut into small rectangular samples approximately 25 mm long, 5−10 mm wide, and 0.100−2 mm thick for DMA tests. DMA tests were performed on a Rheometric Scientific III dynamic mechanical analyzer using RSA Orchestrator v6.58B2 software and 2.0 °C/min ramp rate, 0.1% strain rate, and initial static load of 100−250 g.

Thin film samples for nanointendentation were created by pouring one layer of solution on a glass slide, placing it in a vacuum hood for 24−72 h, and then into a Fisher Scientific Isotemp vacuum oven at 90−140 °C, with vacuum slowly raised to −28 in Hg. Typical thickness of the sample on the slide was 200−1000 μm. Nanoindentation was performed on an MTS Nanoindenter using a DCM indenter head and a Berkovich-shaped diamond indenter operated in batch mode by MTS TestWorks4 controller software. Multiple batch runs with 4−9 offset tests per batch were performed for each sample, and the distance between each test indentation location was set to 20−30 μm in the X and Y directions. The following parameters were set for the test runs: allowable drift = 0.150 nm/s, depth limit = 200−500 nm, frequency target = 0.45 Hz, maximal load = 0.88 mN, Poisson's ratio for PMMA-based systems = 0.375 and for PS-based systems = 0.350. Starting indention locations on the sample for batch runs were chosen randomly but were visually checked via the video viewer to ensure the test did not take place near an air bubble. Batch test results were discarded if any tests within the batch failed.

3. Results and Discussion

3.1. Mechanical Testing Results Summary. To characterize the impact of nanoparticles on the mechanical properties of polymer composites, we used three different mechanical testing techniques: tensile testing, DMA, and nanoindentation. Each technique determines the elastic modulus for the specimen as well as other properties specific to each technique. Nanoindentation is particularly useful in assessing the properties of the interfacial region between the nanoparticles and the surrounding matrix, since this technique probes the local changes in properties that occur on the nanosize scale in the nanocomposite materials. DMA measurements can detect the impact of the presence of nanoparticles on the primary and secondary relaxation processes of polymer chains in their vicinity. Hence, this technique probes the microscale mechanical properties arising from interfacial phenomena at the nanoscale and is indicative of the influence of the local fluctuations of properties. It is important to note that at this size scale the extent of flocculation of the particles in the matrix will have a direct impact on the resulting mechanical properties of the nanocomposite materials. Finally, tensile testing probes the mechanical properties of the polymer nanocomposite at the macroscopic scale. Local phenomena in the vicinity of the nanoparticles are not necessarily expected to translate into changes in the "bulk" properties of the polymers. However, if the volume fraction of the regions that are affected by the local interfacial phenomena is non-negligible, similar changes (at least qualitatively) in properties of the nanocomposites should be observed with all three testing methods.

All samples were prepared using the same procedures, and all mechanical tests were run using the same parameters. This consistent approach to testing provided a true comparison between the reference pure polymer systems, PMMA and PS, and the nanocomposite systems, PMMA−Al_2O_3, PMMA−Fe_3O_4, PS−Al_2O_3, and PS−Fe_3O_4. The combined elastic modulus results of all three testing techniques are shown in Figure 3. While there are quantitative differences between the values of the moduli measured by the different techniques, the overall qualitative trend is the same. The results show a decrease in modulus of the nanocomposite systems as compared to the pure polymer systems. The T_g of the composites were very similar (if not identical) to the T_g of the pure polymers, so the decrease in the moduli upon the introduction of the nanoparticles are not due to a plasticizing effect that the nanoparticles could have exerted on the polymer matrix. These results are inconsistent with the predictions from composite theory, which can account for a possible lowering of the modulus of composites with stiff particles but compliant interphases but suggest that particle fillers are expected to improve the composite's mechanical properties, specifically the elastic modulus, upon effective bonding with the matrix.

3.2. Interphase Characterization. Composite theory assumes perfect interface between the reinforcements and the matrix. If a perfect interface exists, where continuum strain compatibility is present, the composite theory has excellent predictive capabilities. Unfortunately, at the molecular lever, the interface is more complicated and a perfect interface may not even exist. Connections between the polymer matrix and reinforcing particles exist at specific discrete locations where molecules bond with particles, rather than as a continuous interface. The effect of this difference becomes more pronounced when the size of the particles becomes smaller and the interfacial area becomes large. The error created by the assumption of a continuous and compatible interface is larger for a relatively large interface

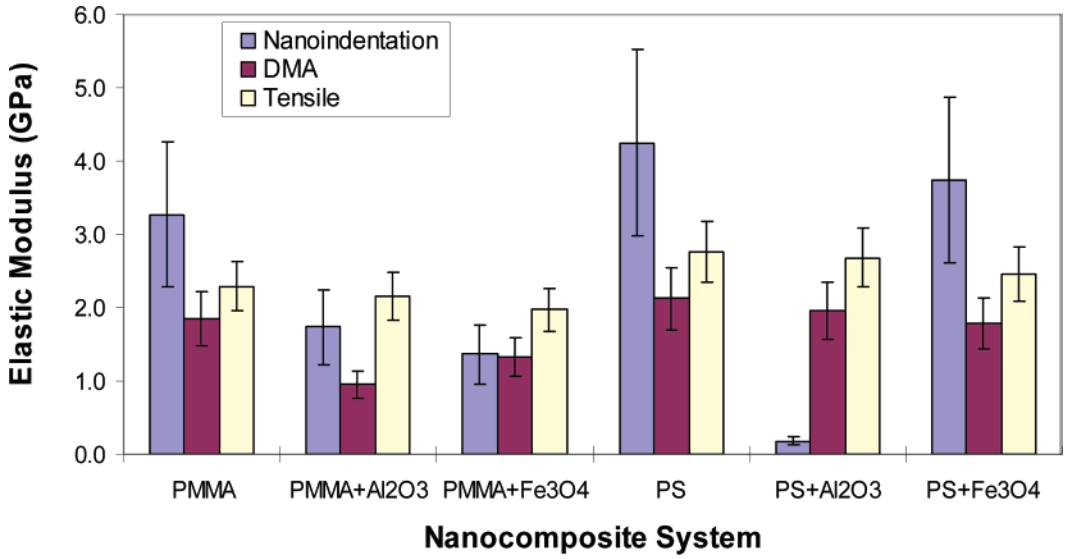

Figure 3. Elastic modulus results for tensile testing, DMA, and nanoindentation mechanical testing.

since, depending on the number of contact points, the actual effective area of bonding between polymer and particles is far less than that of the entire circumferential area of the particle. The actual bonding area depends on the specific polymer−particle system. Since composite theory fails to predict the modulus of our nanocomposites, the logical step is to understand the nature of the interface to identify the degree to which the assumptions in classical composite theory are violated. Since experiments have also shown significant enhancement in modulus for some nanocomposites, it is certainly possible that the classical composite theory assumptions could also predict more accurate results for nanocomposites when the properties of the system are enhanced. Development of a denser interface layer (compared to the matrix) might enhance the effectiveness of the reinforcement particles, thus improving the modulus.

We employed two approaches to characterize the particle−matrix interphase.[26,28,30−32] The first method couples TEM and TGA in order to allow an indirect determination of the average number of polymer segments that are effectively bonded to the metal cluster surface.[31,32] The second method uses the intensity of characteristic infrared bands that are generated as a function of the extent of polymer segment bonding onto the metal cluster surface.[29,30] Unlike previous studies in which these methods have been applied to calculate the extent of interfacial interactions between polymer chains and metal nanoparticles that were formed in situ, here the particles were ready-made and were introduced into the nanocomposite system by the usual filler−matrix mixing techniques. While this procedure allowed for a higher volume fraction of metal clusters to be incorporated into the nanocomposite, it also generated difficulties associated with particle flocculation that were not present in the nanocomposites that were prepared in situ. Moreover, in previous work, the results pertaining to the morphological details of the interfacial region have not been combined with mechanical characterization of those systems to determine the impact of the interphase properties.[32,33]

Although the different interphase characterization techniques take different approaches, they both assume that the structure of the interphase is a function of the nature of the interfacial interactions between the polymer and the reactive sites of the filler surface.[26] Both methods determine the average number of contact points between an adsorbed polymer chain and the nanoparticle. The number of contacts, or anchoring points, per chain indicates the density of polymer layer and thus the density of the interphase. A higher number of contact points per chain means the loops must be smaller so the entire adsorbed chain is closer to the surface and the interphase is denser.[26]

3.2.1. Interphase Characterization Using FTIR. The first interphase characterization approach calculates the density of the interphase by investigating the bonding mechanism in the PMMA-based systems using FTIR. The chemistry behind the interaction of PMMA and aluminum oxide surfaces is well established.[29,30,34] The bonding process between the PMMA chain segments and the aluminum oxide nanoparticle surface is as follows: The aluminum oxide nanoparticle surface molecules react with atmospheric water vapor creating oxy−hydroxide surface groups:

$$Al_2O_3 + H_2O \rightleftarrows 2AlO(OH) \quad (1)$$

This hydration reaction has been proven to occur with several metal oxides, including Al, Cr, Co, and Cu.[29,30,34,35] The presence of the OH group on the nanoparticle surface facilitates hydrolysis of the PMMA ester group to produce either a COOH acid group or its conjugate COO− base group according to the following reaction:[30]

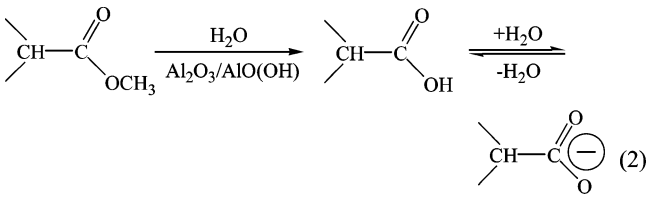

(2)

The COO− group directly interacts with the positively charged Al(III) atoms to generate a bond between the polymer segment and the aluminum oxide nanoparticle surface.[29,30] This bonded segment is an anchoring point for the PMMA chain.

FTIR was performed on the PMMA-capped Fe_3O_4 and Al_2O_3 nanoparticles to confirm that bonding occurs as described above and to translate that information into interphase structure. Previous work has shown that the appearance of specific peaks in the IR spectrum indicates the existence of bonding between PMMA and a metal oxide surface upon polymer adsorption.[29,30,34,35] The summary of the various pertinent infrared

Table 1. Infrared Absorption Bands Resulting from of PMMA Segment Adsorption on Al_2O_3 Surfaces

band, cm^{-1}	change	peak assignment
2950	lower absorbance	O−CH_3 bond is broken
1734	lower absorbance	C═O is no longer isolated
1687	new absorption band	formation of COO− group
1156 and 1171	peak ratio inversion	C−C and C−O stretching modes

absorption bands associated with the reactive adsorption of PMMA onto metal oxide clusters is presented in Table 1. The changes in the infrared spectra of PMMA resulting from its interactions with oxide surfaces are shown in Figure 4. The decrease in the absorbance of the 2950 cm^{-1} peak, corresponding to the hydrolysis of some of the methoxy groups in adsorbed PMMA, is the first stage in the adsorption process, as indicated in the first reaction of eq 2, and is shown in Figure 4a. The second and third reactions of eq 2 are characterized by changes in the absorbances of various bands in the carbonyl region. The relative increase of the 1687 cm^{-1} peak, corresponding to carboxylate groups, as compared to the 1734 cm^{-1} carbonyl peak for the adsorbed PMMA, as shown in Figure 4b, indicates that the predicted bonding process between PMMA and aluminum oxide has indeed taken place. The similarity between the PMMA−Al_2O_3 and PMMA−Fe_3O_4 spectra (not shown) suggests that the adsorption of PMMA on magnetite nanoparticles proceeds via the same mechanism.

Since the carboxylate groups generated in the PMMA chains participate in the bonding to the particle surface, quantifying the number of participating groups can serve as an estimate for the number of bonds. The 1687 cm^{-1} absorption band, shown in Figure 4b (inset), corresponds to the asymmetric stretch of the COO− group, which is indicative exclusively of the COO− group bonding with the surface.[29,30] Evaluating the ratio of the COO− groups participating in bonding (absorbance intensity of the 1687 cm^{-1} peak) to the unreacted carbonyls in the ester groups (absorbance intensity of the 1734 cm^{-1} peak) provides the relative concentration of the reacted COO− group.[29,30] The number of anchoring points for a particular polymer chain is dependent on, and limited by, the chain conformation, length, and strength of interaction with the surface. Therefore, the COO−/C═O ratio may initially increase with the increase in the adsorption layer, but once a monolayer of polymer has been anchored (i.e., chemisorbed), no additional carboxylate groups will be formed, and hence, this ratio will be indicative of the relative concentration of the chains at the interface.

The reactive adsorption of PMMA on the surface of the metal oxide nanoparticles through direct bonding of segments requires a change in the conformation of the polymer at the surface of the nanoparticles.[32,33,36] These conformation rearrangements in the polymer generate a change in the cooperative symmetric and asymmetric stretches of the C−O and C−C bonds of the polymer in the 1100−1200 cm^{-1} spectral region. The shift in the relative intensities of the 1156 and 1171 cm^{-1} infrared absorption bands is very apparent when comparing the PMMA thin film spectrum against the PMMA-capped nanoparticle spectra, as shown in Figure 4c. The ratio of these two bands indicates the proportion of polymer segments that experience the conformational changes indicative of the bonding process. The total number of PMMA carboxylate groups that have undergone hydrolysis and have anchored to the surface can be calculated from the ratio of the fraction of the segments containing the bonding group (COO−) experiencing the conformational change multiplied by the total number of monomers in the sample. Dividing this by the total number of chains gives

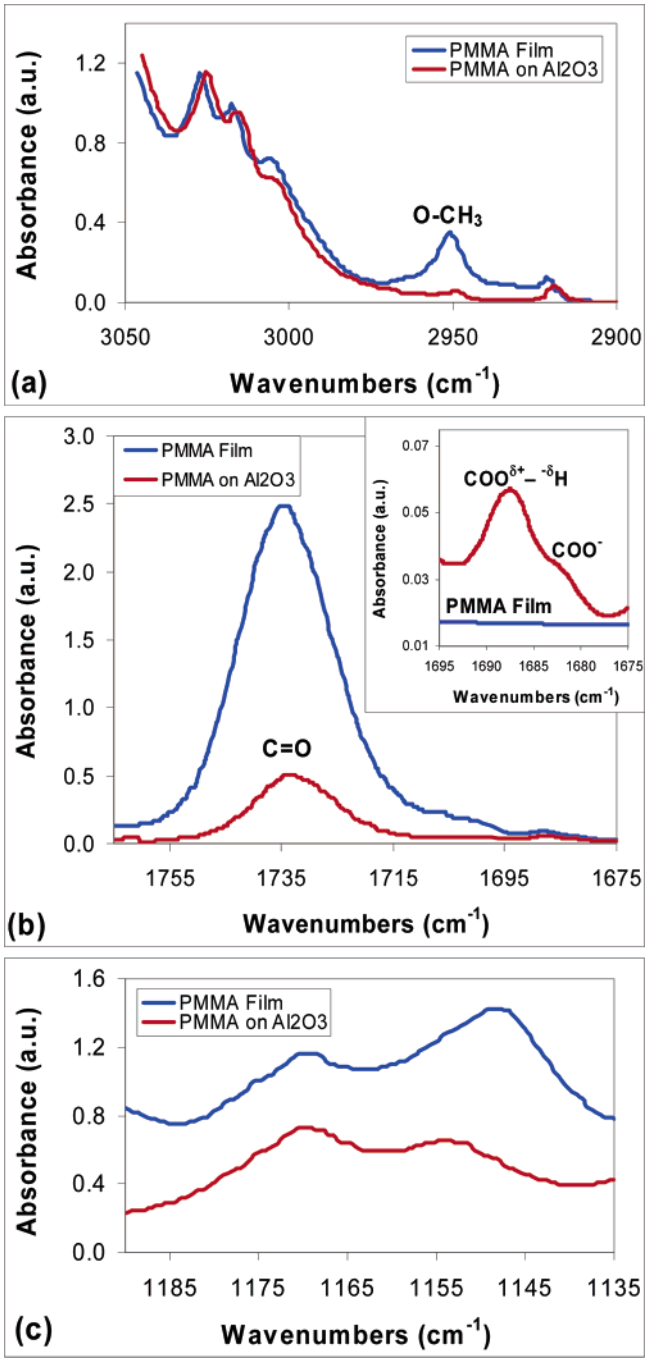

Figure 4. FTIR spectra for the PMMA−Al_2O_3 system: (a) The change in the 2950 cm^{-1} absorption band, indicating the hydrolysis of the O−CH_3 group in adsorbed PMMA. (b) The decrease of the 1734 cm^{-1} absorption band, indicating a change in the bonding properties of the C═O group due to PMMA adsorption and the hydrolysis of the methoxy group. The inset shows the appearance of the 1687 cm^{-1} absorption band, corresponding to the asymmetric stretch of the carboxylate groups (COO−), indicating the formation of a carboxylate-metal bond. (c) FTIR spectra showing the changes in the relative intensities of the 1171 and 1151 cm^{-1} bands corresponding to overlapping C−C and C−O stretching modes in the C−C−O sequence, indicating changes in the conformation of the PMMA due to surface confinement upon adsorption.

the number of anchoring points per chain, according to eq 3:[29,30,34]

$$\text{no. of anchors/chain} = \frac{E_{1687}}{E_{1734}}\frac{E_{1156}}{E_{1171}}\frac{N_{\text{monomers}}}{N_{\text{chains}}} \qquad (3)$$

The total number of monomers in the sample is given by

Table 2. Absorbances from FTIR Spectra and the Calculated Number of Anchors per Chain for the PMMA−Al_2O_3 and PMMA−Fe_3O_4 Systems[a]

	PMMA−Al_2O_3	PMMA−Fe_3O_4
E_{1156}	0.3106	0.3109
E_{1171}	0.4528	0.4502
E_{1687}	0.0315	0.0323
E_{1734}	0.5507	0.5772
N_{chains}	5.31×10^{14}	1.06×10^{15}
$N_{monomers}$	1.85×10^{18}	3.69×10^{18}
anchors/chain	137 ± 12	135 ± 12

[a] Note that only the PMMA-based systems were analyzed by FTIR, since only in these systems a considerable change in the characteristic infrared absorption bands of the polymer could be observed.

$N_{monomers} = \bar{M}_w N_{chains}/M_0$, where M_0 is the molecular weight of the monomer and the total number of chains in the sample is given by $N_{chains} = M_{sample} w_{polymer} N_A/\bar{M}_w$, where M_{sample} is the mass of the sample, $w_{polymer}$ is the mass fraction of polymer as determined from TGA data, and $\bar{M}_w$ is the weight-average molecular weight of the polymer. Using the data from the FT-IR spectra and using eq 3, the number of anchors per chain was calculated for the PMMA-based nanocomposites, as shown in Table 2.

The results in Table 2 are somewhat surprising given those from previous studies,[26] in which the same characterization approach indicated that PMMA chains ($\bar{M}_w = 330\,000$ g/mol) adsorbed on cobalt oxide nanoclusters formed 466 anchoring points per chain per cluster.[26] In these previous studies, the number of anchors per chain was calculated for several different molecular weights of PMMA, showing that with longer, more flexible chains the energetic penalty for the loss of conformational entropy, due to chain confinement on the surface, decreases. Hence, the strong interaction of the polymer with the surface outweighs the entropic loss, and the more flexible chains can form additional anchoring points with the surface.[26] In the present study we used even longer chains of PMMA ($\bar{M}_w = 350\,000$ g/mol), and the expectation was that the resulting number of anchoring points would be even higher. Instead, we obtained 137 and 135 anchoring points for the PMMA−Al_2O_3 and PMMA−Fe_3O_4 nanocomposite systems, about only one-fourth of the actual expected magnitude of anchors per chain. Given the fact that the infrared spectra of both systems show the same type of features, the difference in reactivity between Co_2O_3 and Al_2O_3 or Fe_3O_4 could only partially account for the lower number of anchoring points. It is important to note that the critical difference between the current study and the study involving Co_2O_3 is the fact that the Co_2O_3 nanoparticles were generated in situ via the decomposition of cobalt carbonyls in the presence of PMMA. In this system, the PMMA chains were able to come in contact with the coordinatively unsaturated, reactive, growing metallic fragments, which provided a much greater opportunity for the PMMA chains to adsorb onto the surface. Conversely, in the current study, we utilized preformed nanoparticle clusters that had already been processed and limited to a particular size. The surfaces of these particles are far less reactive and provide less energetic drive for bonding with PMMA.

3.2.2. Interphase Characterization Using TGA and TEM. The FTIR is applicable only to metal−polymer composites in which the interfacial interactions generate considerable changes in the infrared spectrum of the polymer arising from new bonding between the two moieties at the interface. However, for interfacial interaction driven primarily by van der Waals attractions, such as between polystyrene and metal oxide surfaces, a different characterization method was used. The second characterization approach calculated the number of anchoring points using the average cluster size from TEM and the total mass of the polymer directly absorbed on the metal clusters from TGA. Using this information, the structure of the loops and chains can be defined to determine the number of anchoring points. As shown in Figure 2, the interphase boundary extending out from a particle surface is described by the thickness of the polymer layer directly adsorbed onto the particle, L_{eff}. Within the interphase region, the adsorbed polymer chains form loops and trains over the surface. Assuming that the conformation of the polymer in the loops is that of a random coil, it is possible to calculate the minimum number of segments present in a loop, n_{loop}, based on the number of segments n_{eff} in a random coil of length L_{eff}. The number of segments in a loop combined with the molecular weight of the polymer determines the number of anchoring points per chain.

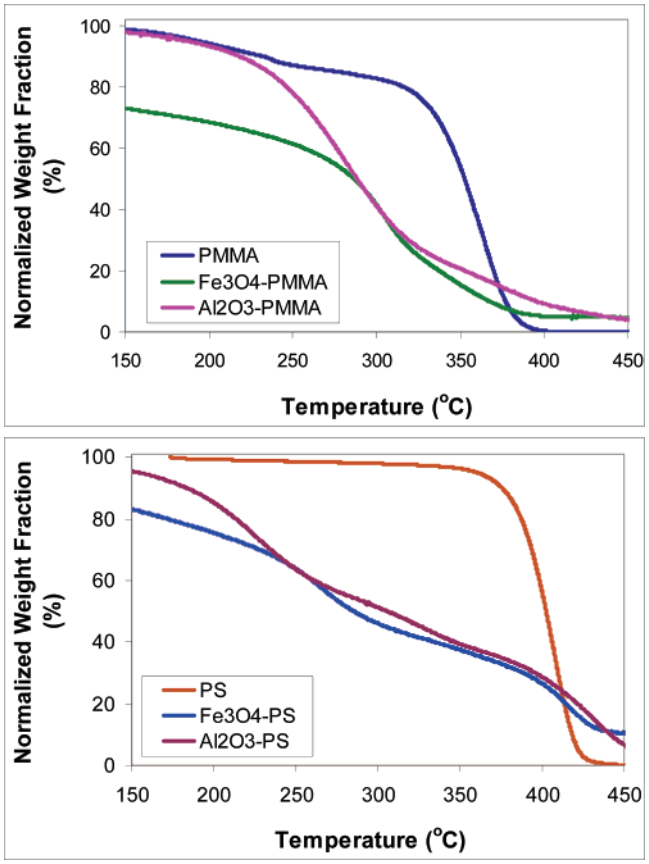

Figure 5. TGA decomposition profiles for the PMMA-based and the PS-based systems.

TGA decomposition data obtained from capped particles determine the weight fraction of the polymer layer adsorbed on the metal oxide particles. The difference between the starting and final weight of the sample represents the weight of the polymer burned off during the experiment. As seen in the PMMA-based system experiments, shown in Figure 5, the polymer layer constituted 9.1% of the PMMA−Al_2O_3 particle mass and 15.1% of the PMMA−Fe_3O_4 particle mass. On the basis of only these data, one might conclude that the Fe_3O_4 surfaces are more reactive with PMMA since more chains anchored to the surface. One important consideration, however, is that more tightly bound chains can shield the surface from other chains, likely resulting in a denser layer formed from fewer number of chains with fewer entanglements with other chains.[26,28] Therefore, this higher weight fraction of bound chains on Fe_3O_4 is likely due to weaker bonding of a larger number of chains

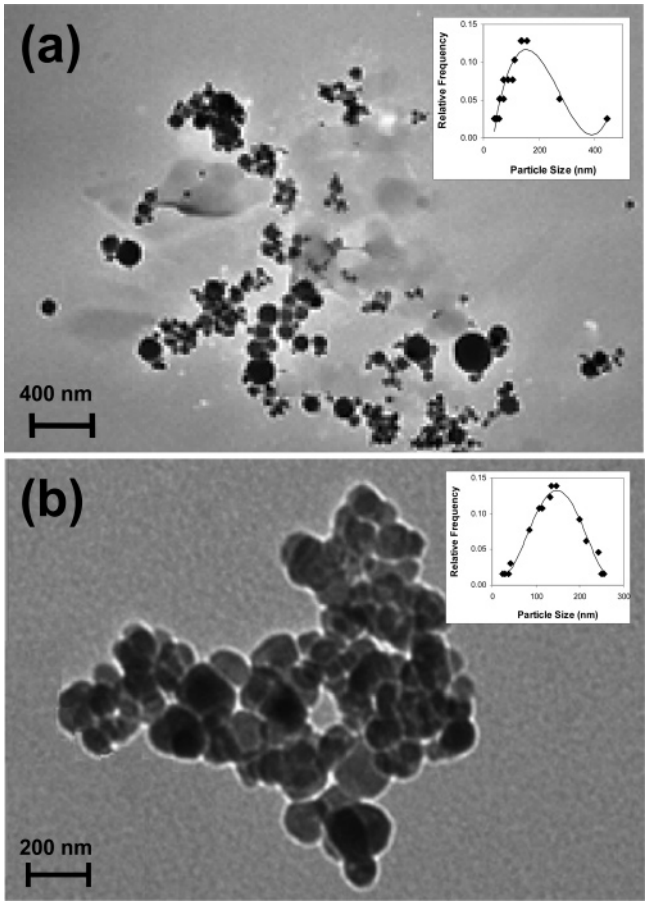

Figure 6. TEM image of the reacted polymer−oxide nanoparticle solution of the PS−Al_2O_3 system (a) and PS−Fe_3O_4. Images were used to measure particle size distribution shown for each system in the upper-right-hand side of each image.

with the surface through fewer number of anchors and a higher degree of entanglements with unbound chains.[33]

The average size of the oxide nanoparticles was determined from TEM images such as the one of the PS−Al_2O_3 sample shown in Figure 6a and PS−Fe_3O_4 in Figure 6b. Particle sizes determined from TEM were 2−3-fold larger than manufacturer stated sizes with large standard deviations indicating the occurrence of particle flocculation. With both the average particle size from TEM and the weight fraction of polymer in the capped-particle sample from TGA, the number of anchoring points per chain can be calculated. The first step is to derive the expression for the thickness of the bound polymer layer around the particles. The thickness of the polymer layer, L_{eff}, is determined by first considering the total volume of a polymer-capped particle, V_{total}. The total volume of the capped particle includes both the metal oxide cluster volume and the volume of the polymer layer bound to the surface, $V_{\text{total}} = V_{\text{cluster}} + V_{\text{polymer}}$. The volume of the polymer adsorbed on the metal oxide cluster can be calculated using the weight fraction of the polymer, the mass of the TGA sample, the number of clusters in the sample (N_{clusters}), and the density of a thin film of polymer (ρ) given as 1.05×10^{-21} g/nm^3 for PS and 1.17×10^{-21} g/nm^3 for PMMA.

$$V_{\text{polymer}} = \frac{M_{\text{sample}} w_{\text{polymer}}}{N_{\text{clusters}} \rho} \tag{4}$$

The number of clusters in the sample is the quotient of the number of oxide molecules in the sample ($N_{\text{molecules}}$) and the number of oxide molecules per cluster ($N_{\text{molecule/cluster}}$), which assumes that the volume fraction of the molecules in the cluster (ϵ) is 0.7.

$$N_{\text{clusters}} = \frac{N_{\text{molecules}}}{N_{\text{molecules/cluster}}} = \frac{\left(\frac{M_{\text{sample}} w_{\text{cluster}} N_{\text{A}}}{M_{\text{molecule}}}\right)}{\epsilon\left(\frac{D_{\text{cluster}}}{d_{\text{molecule}}}\right)^3} \tag{5}$$

The diameter of an oxide molecule was calculated as 0.52 and 0.43 nm for Fe_3O_4 and Al_2O_3, respectively (based on the manufacturer-provided density of each metal oxide).

Assuming spherical clusters, the average diameter of the clusters (D) provides the volume of a metal oxide cluster without an adsorbed polymer layer.

$$V_{\text{cluster}} = \left(\frac{4\pi}{3}\right)\left(\frac{D}{2}\right)^3 \tag{6}$$

The total cluster volume including the adsorbed polymer layer of thickness L_{eff}, is now given by

$$V_{\text{total}} = \left(\frac{4\pi}{3}\right)\left(\frac{D + 2L_{\text{eff}}}{2}\right)^3 \Rightarrow L_{\text{eff}} = \left(\frac{3}{4\pi} V_{\text{total}}\right)^{1/3} - \frac{D}{2} \tag{7}$$

To derive an expression for L_{eff}, we rearrange eq 7 and substitute $V_{\text{cluster}} + V_{\text{polymer}} = V_{\text{total}}$. Simplifying through several steps leads to an expression for L_{eff} that incorporates the TGA and TEM experimental data, as shown in eq 8.[32]

$$L_{\text{eff}} = \frac{1}{2}\left[\frac{6 w_{\text{polymer}} M_{\text{molecule}} \epsilon}{\pi \rho w_{\text{cluster}} N_{\text{A}}}\left(\frac{D}{d_{\text{molecule}}}\right)^3 + D^3\right]^{1/3} - \frac{D}{2} \tag{8}$$

Thus, using the expression for L_{eff}, one can calculate the corresponding average number of repeating units, n_{eff}:

$$n_{\text{eff}} = \frac{1 + \cos\theta}{2(1 - \cos\theta)}\left(\frac{L_{\text{eff}}}{\sigma l}\right)^2 \tag{9}$$

where $\theta = 109.5°$, $l = 1.54$ Å, and the steric hindrance factors, σ, for PS and PMMA are 2.3 and 2.1, respectively.[33] As shown in Figure 2, the minimum number of free repeating units that exist in a loop between two anchoring points, n_{loop}, is given by $n_{\text{loop}} = 2n_{\text{eff}} - 1$. Hence, the number of anchoring points per chain is given by the quotient of the average number segments (monomers) in a chain and n_{loop}:

$$\text{no. of anchors/chain} = \frac{N_{\text{monomers}}}{n_{\text{loop}}} = \frac{\bar{M}_{\text{w}}}{M_{\text{monomer}}(2n_{\text{eff}} - 1)} \tag{10}$$

Using the data gleaned from TGA and TEM and these equations, the number of anchoring points per chain was calculated for all four nanocomposite systems, as shown in Table 3.

The calculated results for adsorbed PS are consistent with previous research.[26,32] The calculated average number of anchors for PS chains ($\bar{M}_{\text{w}} = 250\,000$) on Co_2O_3 nanoclusters using the combined TEM/TGA characterization method was 52.9.[26] Similarly, the average number of anchors for PS chains ($\bar{M}_{\text{w}} = 350\,000$) on Al_2O_3 nanoclusters (obtained from the combined TEM/TGA method) was calculated at 49.7 anchors per chain and for PS chains ($\bar{M}_{\text{w}} = 350\,000$) on Fe_3O_4 nanoclusters was 9.5. Since Al_2O_3 nanoparticles are considered to exhibit higher surface energy than Fe_3O_4 nanoparticles,[37−39] it would be expected that the PS−Al_2O_3 system exhibits a much denser interphase than the PS−Fe_3O_4 system due to more efficient

Table 3. Calculation of Interphase Morphology Using TGA and TEM Experimental Data[a]

	PMMA−Al_2O_3	PMMA−Fe_3O_4	PS−Al_2O_3	PS−Fe_3O_4
D_{avg} (nm)	124	139	135	154
L_{eff} (nm)	4.59	10.92	5.87	9.47
n_{eff}	50.28	284.80	68.59	178.49
n_{loop}	99.55	568.60	136.18	355.98
anchors/chain	35 ± 15	6 ± 25	50 ± 15	10 ± 25

[a] The large errors associated with the calculated number of anchoring points per chain are due to the fact that only a small number of particles was available for size evaluation. Similar sizes were also calculated from SEM images of samples after fracture during tensile testing experiments.

adsorption on the more reactive surface. In the case of PS-based systems, it was not possible to develop an infrared spectroscopic method for the characterization of the extent of interfacial interactions because the physisorption of PS on metal oxide particles does not give rise to changes in the infrared spectrum of the polymer in its adsorbed state. Hence, in this case, only the gravimetric method could be used to calculate the number of anchoring points per chain per cluster.

However, a comparison between the calculated average number of anchoring points for the PMMA-based systems obtained via the FTIR method and the TEM/TGA method is indeed possible and reveals considerable discrepancy. Following the FTIR characterization approach, PMMA ($\bar{M}_w = 350\,000$ g/mol) adsorbed on Al_2O_3 nanoclusters formed 137 anchoring points per chain,[26] while only 35.12 anchors per chain were calculated via the TEM/TGA method. For the PMMA−Fe_3O_4 system, 135 anchoring points per chain were calculated via the FTIR method, while only an average 7 were calculated via the TEM/TGA method. The fact that for both oxide systems the average number of anchoring points per chain is considerably lower than that found for the PMMA−Co_2O_3 system stems from the differences in the reactivity of the particles as a result of their in-situ vs ex-situ synthesis. However, the systematic lower number of anchoring points obtained with the TEM/TGA method stems from the average size of the particles, D, that was used in the calculations of L_{eff}, n_{eff}, and n_{loop} and that was evaluated from the TEM images. Since TEM data provide the net particle size without considering nanoparticle flocculation in the composite, the effective average particle diameter of the individual units that are connected loosely with other nanoparticles will be smaller than that obtained from TEM. In other words, since flocculation does not provide the same intrinsic rigidity in the flocculated particles compared to that within a stable aggregate, the effective size of the particle must be calculated first. To obtain comparable results from calculations based on the TEM/TGA experimental data to match the results from calculations based on the FTIR spectra, the flocculation of particles must be accounted for. The two characterization methods yielded similar results when particle size for the PMMA−Al_2O_3 system was set to 39 nm (as opposed to 124 nm suggested by the TEM images) and for the PMMA−Fe_3O_4 system was set to 64 nm (as opposed to 139 nm suggested by TEM), as summarized in Table 4. These sizes are very similar to the particle sizes specified by the nanoparticle manufacturers. Since FTIR calculations, based *only* on particle−polymer interactions, give accurate results on the number of anchoring points/chain, calculation of an equivalent size of the particle gives us a means of evaluating the flocculation parameter. The ratio between the experimental average cluster diameter obtained from TEM and the calculated average equivalent cluster diameter needed to simultaneously satisfy the interfacial morphology results obtained with both characterization methods for the number of polymer anchoring points per cluster, may give an indication as to the degree of aggregation or flocculation that the oxide particles underwent during the formation and testing of the nanocomposites. Since the number of anchoring points per chain per cluster in a given system is directly related to the number of clusters in a given sample, and this latter depends on the volume of each independent cluster, we decided to formulate a flocculation parameter as $(D_{avg}^{TEM}/D_{avg}^{calc})^3$. There may be, of course, other alternatives for expressing in a quantitative manner the possible flocculation process in these systems. However, while more experiments would be required to potentially establish a more general relationship in this respect, it appears that looking at the differences between TEM-measured diameters and calculated equivalent diameters may turn out to be a very useful approach. One must also keep in mind that the characterization of particle sizes by TEM was performed on samples of the original suspensions, and as is frequently the case with reactive colloidal systems, it indicated the occurrence of flocculation. In addition, SEM and some TEM characterization were performed on samples origination from fractured surfaces, and therefore, it is possible that the larger agglomerated particles are on a weaker surface that fractured during the test while the majority of the particles within the sample are smaller. Conversely, the FTIR approach analyzed a more homogeneous portion of the samples.

Table 4. Comparison of the Average Particles Sizes for the Al_2O_3 and Fe_3O_4 Nanoclusters As Obtained by the Manufacturers, Obtained from Analysis of TEM and SEM Images and Calculated To Satisfy the Theoretical Matching of Calculated Anchoring Points Obtained from the Gravimetric Method and Those Obtained from the Spectroscopic Method

particle	D_{avg} purchased (nm)	D_{avg}^{TEM} exptl (nm)	D_{avg}^{calc} calcd (nm)	$(D_{avg}^{TEM}/D_{avg}^{calc})^3$ aggregation index
Al_2O_3	39	124	39	32.14
Fe_3O_4	90	139	64	10.24

4. Conclusions

The polymer nanocomposite systems in this study, PMMA−Al_2O_3, PMMA−Fe_3O_4, PS−Al_2O_3, and PS−Fe_3O_4, do not provide improved mechanical properties over pure PMMA and PS systems, indicating that an in-situ preparation is necessary for these composites to develop their full potential of mechanical properties. A decrease in elastic modulus for each system was proven with consistent results from tensile testing, DMA, and nanoindentation.

Interphase characterization showed limited interaction between the Al_2O_3 and Fe_3O_4 nanoparticles with either of the polymer matrices, as compared to other studies of similar systems. The low number of anchoring points of polymer chains on the metal oxide surfaces calculated in this study results in a low interphase density in each of the nanocomposite systems. The low interphase density around the high number of nanoparticles results in the decrease of elastic modulus. Using preformed nanoparticle clusters seems to restrict the extent of interactions between the polymer and the particles since the polymer is not present in solution during the initial formation of the highly reactive metallic fragments, as is the case with in-situ synthesis. Moreover, preformed nanoparticles can cause uncontrolled particle flocculation during processing generating large inhomogeneities in the distribution of the nanoparticles in the polymer matrix, which, in turn, give rise to lower elastic moduli. An initial, mostly qualitative, attempt to provide a quantitative correlation between δ, the calculated density of

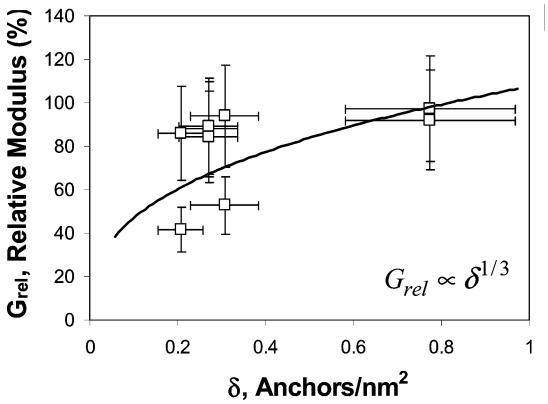

Figure 7. Tentative correlation between the average anchoring points density per nm^2, δ, in a metal oxide−polymer composite and the resulting relative elastic modulus, G_{rel}, the percentage of the elastic modulus of the nanocomposite relative to the elastic modulus of the pure polymer treated in a similar manner but without the embedded nanoparticles, measured by three different mechanical testing methods: tensile stress, DMA, and nanoindentation.

anchoring points per unit area (nm^2), and G_{rel}, the relative elastic moduli of the various systems that were tested (as percentage of the modulus of an identical sample of the pure polymer without the embedded nanoclusters), is shown in Figure 7. It seems that a nonlinear dependence of the moduli on the interfacial morphology is observed, $G_{rel} \propto \delta^{1/3}$, but additional data should be generated before a conclusive correlation could be made. However, this initial attempt provides a road map for the design and implementation of further experiments.

A new way of identifying flocculation is also provided by using correlation data from the FTIR and TEM/TGA methods. Since the number of anchoring points density must be the same irrespective of the methodology and since the FTIR method, which incorporates the particle−polymer interaction, is more accurate than the TEM/TGA results, which cannot define the degree of particle flocculation, an equivalent radius of particles is calculated using the FTIR results. A comparison between this calculated particle radius and that obtained from TEM gives the flocculation parameter that provides a quantitative indication as to the degree of flocculation.

Acknowledgment. This work was supported by the Petroleum Research Fund of the American Chemical Society, PRF #40014-AC5M, and by the Air Force/Bolling AFB/D.C. MURI project on Energetic Structural Materials, Award F49620-02-1-0382.

References and Notes

(1) Vollenberg, P. H. T.; Heikens, D. *Polymer* **1989**, *30*, 1656−1662.
(2) Chan, C.-M.; Wu, J.; Li, J.-X.; Cheung, Y.-K. *Polymer* **2002**, *43*, 2981−2992.
(3) Su, S.; Jiang, D. D.; Wilkie, C. A. *Polym. Adv. Technol.* **2004**, *15*, 225−231.
(4) Park, J. H.; Jana, S. C. *Polymer* **2003**, *44*, 2091−2100.
(5) Gersappe, D. *Phys. Rev. Lett.* **2002**, *89* (5), 058301−1−4.
(6) Reynaud, E.; Jouen, T.; Gauthier, C.; Vigier, G.; Varlet, J. *Polymer* **2001**, *42*, 8759−8768.
(7) Wu, C. L.; Zhang, M. Q.; Rong, M. Z.; Friedrich, K. *Comput. Sci. Technol.* **2002**, *62*, 1327−1340.
(8) Shelley, J. S.; Mather, P. T.; DeVries, K. L. *Polymer* **2001**, *42*, 5849−5858.
(9) Alexandre, M.; Dubois, P. *Mater. Sci. Eng.* **2000**, *28*, 1−63.
(10) Rong, M. Z.; Zhang, M. Q.; Pan, S. L.; Lehmann, B.; Friedrich, K. *Polym. Int.* **2003**, *53*, 176−183.
(11) Shang, S. W.; Williams, J. W.; Soderholm, K.-J. M. *J. Mater. Sci.* **1994**, *29*, 2406−2416.
(12) Brechet, Y.; Cavaille, J.-Y. Y.; Chabert, E.; Chazeau, L.; Dendievel, R.; Flandin, L.; Gauthier, C. *Adv. Eng. Mater.* **2001**, *3*, 571−577.
(13) Jordan, J.; Sharaf, M.; Jacob, K.; Tannenbaum, R.; Jasiuk, I. *Mater. Sci. Eng., A* **2005**, *393*, 1−11.
(14) Zhu, L.; Narh, K. A. *J. Polym. Sci., Part B: Polym. Phys.* **2004**, *42*, 2391−2406.
(15) Ash, B. J.; Rogers, D. F.; Wiegand, C. J.; Schadler, L. S.; Siegel, R. W.; Benicewicz, B. C.; Apple, T. *Polym Comput.* **2002**, *23*, 1014−1025.
(16) Chabert, E.; Bornert, M.; Bourgeat-Lamy, E.; Cavaille, J.-Y.; Dendievel, R.; Gauthier, C.; Putaux, U.; Zaoui, A. *Mater. Sci. Eng., A* **2004**, *381*, 320−330.
(17) Kardos, J. L. *Chem. Innov. (CHEMTECH)* **1984**, *14*, 430−434.
(18) Shia, D.; Hui, C. Y.; Burnside, S. D.; Giannelis, E. P. *Polym. Comput.* **1998**, *19*, 608−617.
(19) Nowicki, W. *Macromolecules* **2002**, *35*, 1424−1436.
(20) Kovacevic, V.; Leskovac, M.; Lucic, B. S. *J. Adhes. Sci. Technol.* **2002**, *16*, 1915−1929.
(21) Vollenberg, P. H. T.; Heikens, D. *J. Mater. Sci.* **1990**, *25*, 3089−3095.
(22) Skau, K. I.; Blokhuis, E. M. *Macromolecules* **2003**, *36*, 4637−4645.
(23) Aubouy, M.; Raphael, E. *Macromolecules* **1998**, *31*, 4357−4363.
(24) Petrovic, Z. S.; Javni, I.; Wasson, A.; Banhegyi, G. *J. Appl. Polym. Sci.* **2000**, *76*, 133−151.
(25) Kovacevic, V.; Lucic, S.; Leskovac, M. *J. Adhes. Sci. Technol.* **2002**, *16*, 1343−1365.
(26) Tannenbaum, R.; Zubris, M.; David, K.; Ciprari, D.; Jacob, K.; Jasiuk, I.; Dan, N. *J. Phys. Chem. B* **2005**, *110*, 2227−2232.
(27) Bolhuis, P. G.; Louis, A. A.; Hansen, J.-P. *Phys. Rev. Lett.* **2002**, *89*, 128302.
(28) Lipatov, Y. S. *Polymer Reinforcement*; ChemTec Publishing: Ontario Canada, 1995; p 385.
(29) Kostandinidis, F.; Thakkar, B.; Chakraborty, A. K.; Potts, L.; Tannenbaum, R.; Tirrell, M.; Evans, J. *Langmuir* **1992**, *8*, 1307−1317.
(30) Tannenbaum, R.; King, S.; Lecy, J.; Tirrell, M.; Potts, L. *Langmuir* **2004**, *20*, 4507−4514.
(31) Hariharan, R.; Russell, W. B. *Langmuir* **1998**, *14*, 7104.
(32) Tadd, E.; Zeno, A.; Zubris, M.; Dan, N.; Tannenbaum, R. *Macromolecules* **2003**, *36*, 6497−6502.
(33) Tannenbaum, R.; Zubris, M.; Goldberg, E. P.; Reich, S.; Dan, N. *Macromolecules* **2005**, *38*, 4254−4259.
(34) King, S.; Hyunh, K.; Tannenbaum, R. *J. Phys. Chem. B* **2003**, *107*, 12097−12104.
(35) Tannenbaum, R.; Hakanson, C.; Zeno, A. D.; Tirrell, M. *Langmuir* **2002**, *18*, 5592−5599.
(36) David, K.; Tannenbaum, R.; Dan, N. *Abstr. Pap. Am. Chem. Soc. 229* **2005**, *607*, *COLL Part 1*, U744−U744.
(37) Gilmore, K.; Idzerda, Y. U.; Klem, M. T.; Allen, M.; Douglas, T.; Young, M. *J. Appl. Phys.* **2005**, *97*, 10B301.
(38) Navrotsky, A. *Geochem. Trans.* **2003**, 34−37.
(39) Jolivet, J.-P.; Froidefond, C.; Pottier, A.; Chaneac, C.; Cassaignon, S.; Tronc, E.; Euzen, P. *J. Mater. Chem.* **2004**, *14*, 3281−3288.

MA0602270